Journal of the Korean Physical Society, Vol. 74, No. 12, June 2019, pp. 1112∼1118

Will a Wiener Filter Decrease the Accuracy of HRTEM Displacement Measurements of Aperiodic Structures?

Gen Li, Dongsheng Song, Zhenyu Liao and Jing Zhu*

National Center for Electron Microscopy in Beijing, School of Materials Science and Engineering, The State Key Laboratory of New Ceramics and Fine Processing, Key Laboratory of Advanced Materials (MOE), Tsinghua University, Beijing 100084, People's Republic of China

(Received 25 February 2019)

Modern Cs-corrected high-resolution transmission electron microscopy (HRTEM) has pushed the resolution limit to sub-angstrom scale and has made possible the quantitative analyses of local aperiodic atomic structures. After images have been obtained, a Wiener filter is often used to improve the signal-to-noise ratio, especially for those samples containing both crystal and large amorphous components. However, a Wiener filter may introduce distortions in the original experimental images. From this point of view, having a fundamental understanding of the effect of a Wiener filter on the accuracy of atomic displacement measurements in aperiodic structures is important. In this work, we first review the principle of the Wiener filter and theoretically discuss the origin of the distortions induced in aperiodic structures by using a Wiener filter. Then, using hypothetical experimental systems that contains both aperiodic crystal structures and amorphous layers, we carried out synthetic experiments to quantitatively estimate the effect of the Wiener filter on the measurements of aperiodic displacements. Compared with the values for a non-filtered image, the signal-to-noise ratio was significantly improved, and the accuracy of the displacement measurement was not decreased when proper Wiener filter parameters were used. Such results are of great importance for the processing of HRTEM images.

PACS numbers: 07.78.+s
Keywords: Wiener filter, Aperiodic structure, Atomic displacement, Quantitative measurement, HRTEM
DOI: 10.3938/jkps.74.1112

I. INTRODUCTION

Since the beginning of the twenty-first century, aberration-corrected transmission electron microscopy has significantly pushed the resolution limit to sub-angstrom scale. With the help of advanced electron microscopes and Gaussian peak-finding techniques, picometer-level measurements of atom positions can be realized, which makes possible the quantitative analysis of local properties and structures on the atomic scale, especially aperiodic structures such as surface reconstructions of oxides [1–4]; local structures near ferroelectric domain walls in $Pb(Zr_xTi_{1-x})O_3$ [5,6], $BiFeO_3$ [7] and $PbTiO_3$ [8,9]; spontaneous vortex ferroelectric domains [10–13]; polar nanoregions of relaxed ferroelectrics [14–16]; and ferroelectric polarization related to thickness and local structures [17–19]. These results provide us with a new angle of view to study materials and deepened our understanding of the relationship between structures and properties.

Generally speaking, if the signal-to-noise ratio (SNR) of the original image is poor, a proper image filter process might be necessary before quantitative measurement. Two filter modes, spatial filters and frequency domain filters, are commonly used. Spatial filters mainly refer to Gauss smearing and mean filters, and frequency filters includes the Wiener filter, the average background subtraction filter (ABS filter), *etc* [20]. Spatial filters deal with the neighborhood of each point, and the distribution of bright points in the image is retained, but they do not work very well for images with strong noise. Frequency domain filters can tolerate larger noise but enhance periodic signals, which introduces additional distortions.

However, some ferroelectrics, such as $(1-x)PbMg_{1/3}Nb_{2/3}O_3{-}xPbTiO_3$ and $Bi_{0.5}Na_{0.5}TiO_3$, can easily to be charged under the illumination of an electron beam, resulting in sample drift and even fracture. Conducting amorphous carbon of 2 to 3 nm in thickness is usually plated to avoid such charging effects [21], despite the new strong noise contributed from the surface layer, which makes the filter process indeed necessary. From this point of view, having a fundamental understanding of possible distortions caused by Wiener filter in aperiodic structure is of importance to analyze high-resolution

*E-mail: jzhu@mail.tsinghua.edu.cn; Tel: +86 010-62794026

images quantitatively, especially measurements of atomic displacements.

In this work, we will first review the principle of the Wiener filter and theoretically discuss the origin of distortions in the aperiodic structure by the Wiener filter. Then, using three hypothetical experimental systems that contains both aperiodic crystal structures and amorphous layers, we carry out synthetic experiments to estimate quantitatively the effect of the Wiener filter on the measurement of the aperiodic displacements.

II. THEORETICAL ANALYSIS

1. Principle of the Wiener filter

For a thin sample with both crystal and amorphous components, assuming weak phase body approximation is satisfied, the electron wave function at the exit surface of the specimen is

$$\psi(\boldsymbol{r}) = 1 - i\sigma(V_c(\boldsymbol{r})t_c + V_a(\boldsymbol{r})t_a), \tag{1}$$

where V_c and V_a are the projected potentials of the crystalline and the amorphous materials, respectively, t_c and t_a are the corresponding thicknesses, and σ is the interaction constant. An additional phase factor $\chi(\boldsymbol{u})$ appears in the frequency domain after passing the object lens, which includes the components of the aberrations. Then, the wave function can be written as

$$\begin{aligned}\phi(\boldsymbol{u}) &= \delta(\boldsymbol{u}) - i\sigma(V_c(\boldsymbol{u})t_c + V_a(\boldsymbol{u})t_a)e^{i\chi(\boldsymbol{u})} \\ &\approx \delta(\boldsymbol{u}) + \sigma(V_c(\boldsymbol{u})t_c + V_a(\boldsymbol{u})t_a).\end{aligned} \tag{2}$$

The approximation in Eq. (2) requires $\sin\chi \approx 1$, which can be roughly satisfied under the so-called Lentzen condition in negative spherical aberration imaging of modern high-resolution transmission electron microscopy (HRTEM):

$$\Delta f = \sqrt{\frac{4}{3}|C_s|\lambda}, \tag{3}$$

here, C_s is the spherical aberration coefficient, and λ is the wavelength of the electron beam. The corresponding spatial wave function in image space is

$$\psi(\boldsymbol{r}) = 1 + \sigma(V_c(\boldsymbol{r})t_c + V_a(\boldsymbol{r})t_a). \tag{4}$$

The image recorded is the product of spatial wave function $\psi(\boldsymbol{r})$ and its complex conjugate

$$\begin{aligned}I(\boldsymbol{r}) &= \psi^*(\boldsymbol{r})\psi(\boldsymbol{r}) \approx 1 + 2\sigma(V_c(\boldsymbol{r})t_c + V_a(\boldsymbol{r})t_a) \\ &= 1 + I_c(\boldsymbol{r}) + I_a(\boldsymbol{r}),\end{aligned} \tag{5}$$

and its Fourier transform is

$$\begin{aligned}F(\boldsymbol{u}) &= \delta(\boldsymbol{u}) + 2\sigma(V_c(\boldsymbol{u})t_c + V_a(\boldsymbol{u})t_a) \\ &\equiv \delta(\boldsymbol{u}) + F_c(\boldsymbol{u}) + F_a(\boldsymbol{u}).\end{aligned} \tag{6}$$

One should note that the $F(\boldsymbol{u})$ here is a complex function. In the process of the Wiener filter, only the last two terms of Eq. (6) need to be considered because the value of $\delta(\boldsymbol{u})$ is zero except at the origin.

The core idea of the Wiener filter is to find an estimate function $\Theta(\boldsymbol{u})$ that would make the difference between the Fourier transform of the crystal sample signal $F_c(\boldsymbol{u})$ and its estimated function $F_c^{est}(\boldsymbol{u})$ as small as possible:

$$F_c^{est}(\boldsymbol{u}) = F(\boldsymbol{u})\Theta(\boldsymbol{u}). \tag{7}$$

When the criterion that the sum of squared residuals should take minimum value is used, namely, $F_c^{est}(\boldsymbol{u})$ makes the sum

$$\begin{aligned}&\sum_u |F_c^{est}(\boldsymbol{u}) - F_c(\boldsymbol{u})|^2 \\ &= \sum_u |(F_c(\boldsymbol{u}) + F_a(\boldsymbol{u}))\Theta(\boldsymbol{u}) - F_c(\boldsymbol{u})|^2,\end{aligned} \tag{8}$$

take a minimum value, one has a Wiener filter. The corresponding estimate function is [20]

$$\Theta_{WF}(\boldsymbol{u}) = \frac{|F_c(\boldsymbol{u})|^2}{|F_c(\boldsymbol{u})|^2 + |F_a(\boldsymbol{u})|^2}. \tag{9}$$

$F_c(\boldsymbol{u})$ and $F_a(\boldsymbol{u})$ are almost orthogonal in the frequency domain; hence, we have the following approximation:

$$|F(\boldsymbol{u})|^2 \approx |F_c(\boldsymbol{u})|^2 + |F_a(\boldsymbol{u})|^2. \tag{10}$$

Then, Eq. (8) can be written as

$$\Theta_{WF}(\boldsymbol{u}) \approx \frac{|F(\boldsymbol{u})|^2 - |F_a(\boldsymbol{u})|^2}{|F(\boldsymbol{u})|^2}, \tag{11}$$

and the estimated crystal signal of the Wiener filter in the frequency domain is

$$\begin{aligned}F_c^{est}(\boldsymbol{u}) &= F(\boldsymbol{u})\Theta_{WF}(\boldsymbol{u}) \\ &= F(\boldsymbol{u})\frac{|F(\boldsymbol{u})|^2 - |F_a(\boldsymbol{u})|^2}{|F(\boldsymbol{u})|^2}.\end{aligned} \tag{12}$$

What remains is to estimate $|F_a(\boldsymbol{u})|$. In fact, because $F_c(\boldsymbol{u})$ is strongly localized around some specific points (corresponding to diffraction spots) in the frequency domain, the intensity between these points mainly comes from the contribution of $F_a(\boldsymbol{u})$. If n-fold aberrations are neglected, $F_a(\boldsymbol{u})$ can be assumed to possess radial symmetry.

In a circle (more precisely a very narrow ring) with radius $|\boldsymbol{u}|$, the brightest pixels correspond to diffraction spots (if some diffraction spots lie on this circle), and dim pixels mainly correspond to the amorphous layer. After drawing the brightness distribution histogram of all the pixels in this circle (or ring) and sorting all the brightness values from the lowest to the highest, we can choose some proper statistic parameters, such as the average intensity $\langle|F(\boldsymbol{u})|\rangle$ or the median intensity of the brightness distribution histogram as an estimate of $|F_a(\boldsymbol{u})|$. In this work,

Table 1. Calculated $\bar{\eta}$ under different R_0 and u_0.

	0.5	1	1.5	2	2.5	3	3.5	4	4.5	5
1	0.35	−0.13	0.030	0.035	−0.080	0.11	−0.13	0.15	−0.16	0.16
2	−0.23	−0.090	−0.020	0.025	0.058	0.081	0.097	0.11	0.11	0.115
3	0.18	−0.071	0.016	0.021	−0.047	0.066	−0.080	0.089	−0.094	0.095
4	−0.15	−0.061	−0.014	0.018	0.041	0.058	0.070	0.077	0.082	0.083
5	0.13	−0.054	0.012	0.016	−0.037	0.052	−0.063	0.070	−0.073	0.074
6	−0.12	−0.049	−0.011	0.015	0.034	0.047	0.057	0.064	0.067	0.068
7	0.11	−0.045	0.0098	0.014	−0.031	0.044	−0.053	0.059	−0.062	0.063
8	−0.10	−0.042	−0.0091	0.013	0.029	0.041	0.050	0.055	0.058	0.059
9	0.096	−0.039	0.0086	0.012	−0.028	0.039	−0.047	0.052	−0.055	0.056
10	−0.09	−0.037	−0.0081	0.012	0.026	0.037	0.045	0.050	0.052	0.053

we chose three quantile fractile, 30%, 50% (the median intensity) and 90%, as estimates of $|F_a(\boldsymbol{u})|$, which correspond to the three so-called different filter strengths, namely, weak, normal and strong, in the MacTempas software.

2. Effect of aperiodic signals

We have already introduced some basic principles of the Wiener filter. Here we will qualitatively analyze how the corresponding Fourier transform image will change when the crystal sample contains an aperiodic signal.

We denote the image intensity of a perfect crystal as $I(\boldsymbol{r})$ and its Fourier transform as $F(\boldsymbol{u})$. We assume that the intensity distribution of each atom on $I(\boldsymbol{r})$ obeys the Gaussian function $g(\boldsymbol{r}) = \exp(-ar^2)$ and that the corresponding Fourier transform is $G(\boldsymbol{u}) = \exp\frac{-u^2}{4a}$.

In the following discussion, only a "weak perturbation" will be discussed, which means the locations of the atoms derivate only slightly from the perfect periodic lattice site; furthermore, no point or line defects such as dislocations and stacking faults will be considered. Because any displacement distribution can be written as the sum of one periodic distribution and one aperiodic distribution whose displacement summation is zero, discussing only the latter situation is reasonable. For simplicity, one pair of atoms in centrally symmetrical positions is assumed to possess displacements with the same lengths but opposite directions: the atom in position $\boldsymbol{R_m}$ moves to position $\boldsymbol{R_n}$, and the atom in position $-\boldsymbol{R_m}$ moves to position $-\boldsymbol{R_n}$. The intensity of the new image can be written as

$$\begin{aligned} I'(\boldsymbol{r}) &= I(\boldsymbol{r}) - g(\boldsymbol{r}) * \delta(\boldsymbol{r}-\boldsymbol{R_m}) + g(\boldsymbol{r}) * \delta(\boldsymbol{r}-\boldsymbol{R_n}) \\ &\quad -g(\boldsymbol{r}) * \delta(\boldsymbol{r}+\boldsymbol{R_m}) + g(\boldsymbol{r}) * \delta(\boldsymbol{r}+\boldsymbol{R_n}) \\ &= I(\boldsymbol{r}) - g(\boldsymbol{r}-\boldsymbol{R_m}) + g(\boldsymbol{r}-\boldsymbol{R_n}) - g(\boldsymbol{r}+\boldsymbol{R_m}) \\ &\quad +g(\boldsymbol{r}+\boldsymbol{R_n}), \end{aligned} \tag{13}$$

and the corresponding Fourier transform is

$$\begin{aligned} F'(\boldsymbol{u}) = F(\boldsymbol{u}) &- \exp(2\pi i \boldsymbol{R_m}\cdot\boldsymbol{u})G(\boldsymbol{u}) \\ &+ \exp(2\pi i \boldsymbol{R_n}\cdot\boldsymbol{u})G(\boldsymbol{u}) \\ &- \exp(-2\pi i \boldsymbol{R_m}\cdot\boldsymbol{u})G(\boldsymbol{u}) \\ &+ \exp(-2\pi i \boldsymbol{R_n}\cdot\boldsymbol{u})G(\boldsymbol{u}). \end{aligned} \tag{14}$$

Here, $\boldsymbol{R_n} = \boldsymbol{R_m} + \boldsymbol{d}$, where $\boldsymbol{d}$ is the atomic displacement vector, and its length usually is on the order of one-tenth the unit cell constant. Then, Eq. (14) can be simplified as

$$\begin{aligned} &F'(\boldsymbol{u}) \\ &= F(\boldsymbol{u}) + 2\cos[2\pi(\boldsymbol{R_m}+\boldsymbol{d})\cdot\boldsymbol{u}]G(\boldsymbol{u}) \\ &\quad - 2\cos[2\pi\boldsymbol{R_m}\cdot\boldsymbol{u}]G(\boldsymbol{u}) \\ &= F(\boldsymbol{u}) - 4\sin[2\pi(\boldsymbol{R_m}+\frac{\boldsymbol{d}}{2})\cdot\boldsymbol{u}]\sin(\pi\boldsymbol{d}\cdot\boldsymbol{u})G^2(\boldsymbol{u}), \end{aligned} \tag{15}$$

and the intensity distribution of the new Fourier transform is

$$\begin{aligned} &|F'(\boldsymbol{u})| \\ &\approx |F(\boldsymbol{u})| - 4\sin[2\pi(\boldsymbol{R_m}+\frac{\boldsymbol{d}}{2})\cdot\boldsymbol{u}]\sin(\pi\boldsymbol{d}\cdot\boldsymbol{u})G^2(\boldsymbol{u}) \\ &= |F(\boldsymbol{u})| - F_d(\boldsymbol{u}). \end{aligned} \tag{16}$$

$|F(\boldsymbol{u})|$ in Eq. (16) is the original Fourier transform, and $F_d(\boldsymbol{u})$ stands for the intensity change caused by atomic displacement, which may be positive or negative. As mentioned above, proper quantile fractile of the intensity distribution along a circle with radius $|\boldsymbol{u}|$ can be used as an estimate of $|F_a(\boldsymbol{u})|$ because $F_a(\boldsymbol{u})$ can be assumed to have radial symmetry, but $F_d(\boldsymbol{u})$ does not possess radial symmetry. If the integral of $F_d(\boldsymbol{u})$ is zero along the circle, the sum of $|F'(\boldsymbol{u})|$ will also be the sum of $|F_a(\boldsymbol{u})|$, which means that the amorphous intensity $F_a(\boldsymbol{u})$ will be removed while $|F(\boldsymbol{u})|$ and $F_d(\boldsymbol{u})$ will be preserved after the filter process; therefore, the filtered image will only contain the lattice signal and the displacement signal. On the other hand, if the integral of

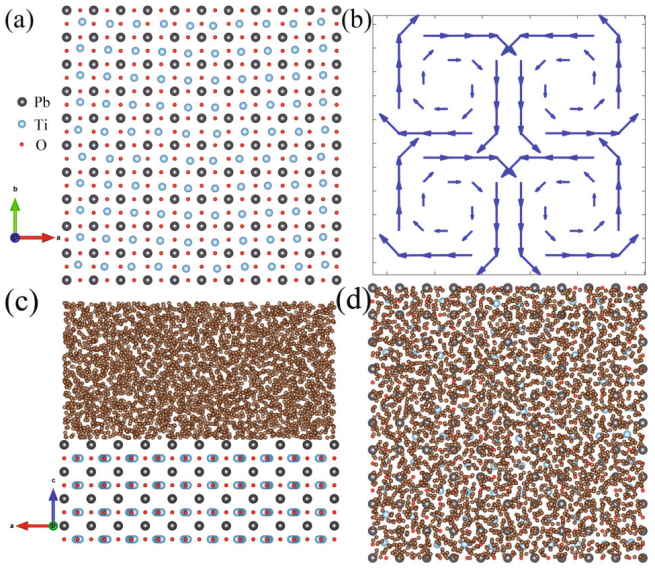

Fig. 1. (Color online) (a) Vertical view of the superlattice used in the synthetic experiments and (b) corresponding displacement distribution of B-site Ti ions in (a). (c) Lateral and (d) vertical views of the superlattice used in the synthetic experiments with 2 nm amorphous carbon.

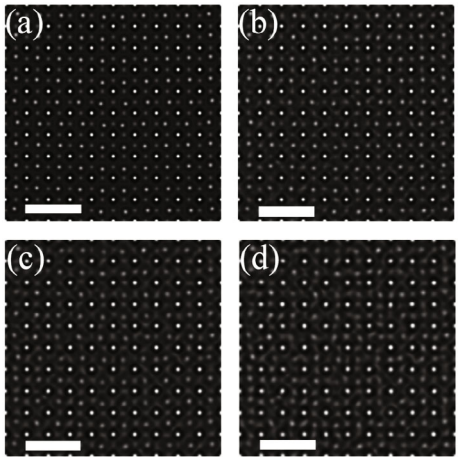

Fig. 2. (a) Simulated image of the superlattice, and (b)–(d) simulated images of amorphous carbon with thicknesses of 2 nm, 4 nm and 6 nm, respectively. The scale bar is 1 nm.

$F_d(\boldsymbol{u})$ is not zero, some displacement information will also be removed. From this point of view, using

$$\eta = \frac{\int_{|\boldsymbol{u}|=u_0} F_d(\boldsymbol{u}(\theta))d\theta}{\int_{|\boldsymbol{u}|=u_0} |F_d(\boldsymbol{u}(\theta))|d\theta}, \tag{17}$$

to describe qualitatively the loss of aperiodic displacement information after the filter is reasonable. The closer η is to zero, the smaller is the effect of the Wiener filter on the aperiodic lattice information.

For a simple estimate, we assume the original image to be that of a cubic lattice and use $\boldsymbol{d} = 0.1\boldsymbol{a_x} + 0.1\boldsymbol{a_y}$, $\boldsymbol{u} = (u_0 \cos\theta \boldsymbol{u_x},\ u_0 \sin\theta \boldsymbol{u_y})$, and $\boldsymbol{R_m} = (R_0 \cos\alpha \boldsymbol{a_x}, R_0 \sin\alpha \boldsymbol{a}_y)$. Here, $\boldsymbol{a_x}$ and $\boldsymbol{a}_y$ are lattice vectors along two directions, $\boldsymbol{u}_x$ and $\boldsymbol{u}_y$ are two corresponding unit vectors in the frequency domain, and u_0 and R_0 are scalar values. For each chosen α, the corresponding η can be calculated and if the impact of different directions of $\boldsymbol{R_m}$ is to be considered, the average $\bar{\eta}$ must be calculated under different α angles.

In our numerical calculations, $\theta \in (0, 2\pi)$, $\alpha \in (0, \pi)$, R_0 ranges from 1 to 10, and u_0 ranges from 0.5 to 5. Calculated results of $\bar{\eta}$ are shown in the following Table 1. The table shows that the absolute value of $\bar{\eta}$ is large only when u_0 is very small ($u_0 = 0.5$) and that the absolute values are not more than 0.16 in the other cases. Furthermore, the absolute value of $\bar{\eta}$ tends to decrease when u_0 and R_0 increase. Hence, for a given image that contains both amorphous noise and aperiodic displacement information, the latter will remain to some degree after the Wiener filter, and the low frequency component will experience relatively more loss. If the degree of distortion of aperiodic displacement information is to be further explored, a series of simulation experiments are necessary.

III. SYNTHETIC EXPERIMENT AND DISCUSSION

A virtual superlattice that contains 1600 atoms is built. In Fig. 1(a), the black circles are lead atoms, the blue ones are titanium atoms, and the red ones are oxygen atoms. The basic unit of this supercell is a cubic lattice similar to a perovskite structure with a lattice constant 0.4 nm. The oxygen atoms collinear with the titanium atoms are removed to form a clear atomic image of Ti columns; otherwise, the image of shifted Ti columns will be elliptical because of the overlap with unshifted oxygen atoms, which is not beneficial for a quantitative analysis. The cubic lattice is then repeated 10 times along the a axis, 10 times along the b axis and 4 times along the c axis to obtain the supercell. In order to reflect the aperiodic displacement, inspired by Yadav's work on the polar vortices in oxide superlattice [13], we added ferroelectric displacements with different lengths and directions for B-site titanium atoms. Their distribution forms one clockwise vortex and one anti-clockwise vortex structure. As shown in Fig. 1(b), the sum of these atomic displacement vectors is zero, and the largest displacement length is 40 pm. Next, we added a series of amorphous carbon layers with thicknesses 2 nm, 4 nm and 6 nm over the original lattice model to simulate practical situations. The original amorphous carbon model of thickness was first equilibrated at high temperatures of about 10000 K for 50 ps to obtain a disordered structure,

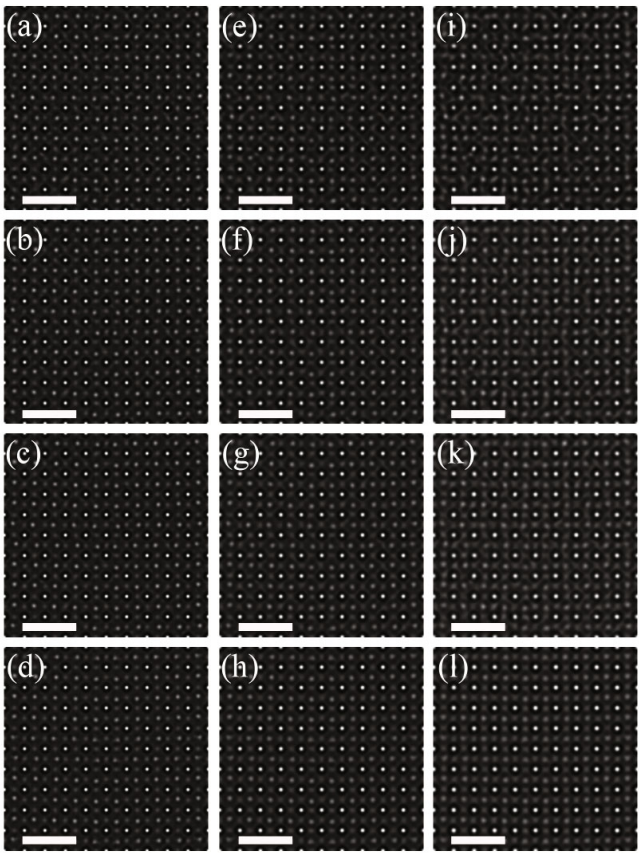

Fig. 3. Wiener filtered images. Wiener filter results of a model with (a)–(d) a 2-nm, (e)–(h) a 4-nm, and (i)–(l) a 6-nm amorphous layer. Rows 1–4 correspond to filter quantile fractiles of 0, 30%, 50% and 90%, respectively. The scale bar is 1 nm.

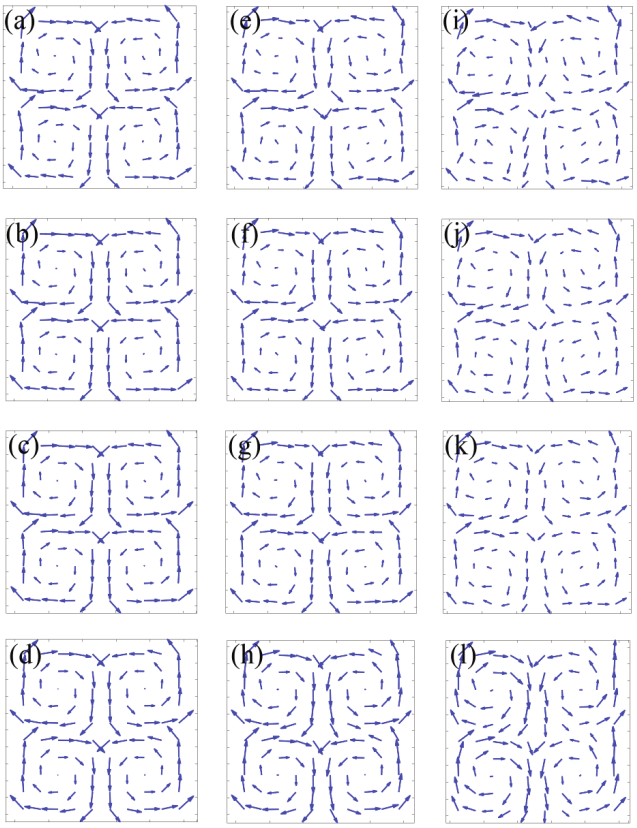

Fig. 4. (Color online) Displacement distributions of B-site ions corresponding to Fig. 3. Wiener filter results of a model with (a)–(d) a 2-nm, (e)–(h) a 4-nm, and (i)–(l) a 6-nm amorphous carbon layer. Rows 1-4 correspond to quantile fractiles of 0, 30%, 50% and 90%, respectively, used in the Wiener filter process.

and was then quenched to 298 K and kept at that temperature for about 10 ps to adjust the atomic positions slightly, as introduced in Ref. 22. Models for thicknesses of 2 nm and 6 nm were made by slicing and splicing the original model. Figures 1(c) and 1(d) show lateral and vertical views of the superlattice with a 2-nm-thick amorphous carbon layer.

The MacTempas software was used to simulate TEM images under different thicknesses and defocus. The following optimal imaging conditions were selected: spherical aberration coefficient $C_3 = -0.0136$ mm and an objective lens over-focus $\Delta f = 5$ nm, which corresponds to the Lentzen condition in negative spherical aberration imaging as shown in Eq. (3). Under such imaging conditions, atoms are sharp, bright spots in a black background with good contrast and can be accurately located by Gaussian fitting. Corresponding simulation images are shown in Fig. 2, where Fig. 2(a) is the simulated image of the pure superlattice, and Figs. 2(b)–(d) are simulated image for amorphous layer thicknesses of 2 nm, 4 nm and 6 nm, respectively. All the simulations were made using the multi-slice method, in which the electron wave will first propagate through the amorphous layer and then through the crystal. The size of simulated images is 512 × 512, which corresponds to a pixel size of about 8 pm and is comparable with experimental conditions. In order to control variables, we only used optimal parameters for our simulation; we do not discuss other factors such as the axis tilt or astigmatism.

The Wiener filter process for an image with noise of an amorphous carbon layer was done by using MacTempas software, followed by Gaussian peak fitting to determine atomic positions. Three estimate parameters, namely, 30%, 50% and 90% quantile fractiles of the brightness distribution histogram, were applied in the Wiener filter process as estimates of $|F_a(\boldsymbol{u})|$, and the corresponding filter results are shown in Fig. 3. The spots in images with a thin amorphous carbon layer can be seen to be round and sharp, while those in images with a thick amorphous carbon layer are a little blurred and distorted; after the Wiener filter, the quality of the images was greatly improved.

Furthermore, we can draw the displacement distribution mappings of B-site ions relative to the center of the

Table 2. Length and angle deviation of B-site atoms under different conditions.

Amorphous	$\overline{L_a}$ (pm)				$\overline{L_r}$ (%)				$\overline{A}$ (°)			
thickness	0	30%	50%	90%	0	30%	50%	90%	0	30%	50%	90%
2 nm	2.7	2.5	2.6	4.6	7.9	7.3	7.7	13.3	4.9	3.5	3.1	3.6
4 nm	4.0	3.6	3.9	7.9	12.6	11.2	12.0	21.9	7.6	5.6	4.8	6.4
6 nm	7.7	7.0	7.5	14.8	22.9	20.9	22.1	42.2	15.4	11.3	10.0	12.6

four nearest A-site ions by using MATLAB to depict the displacement distortion induced by the Wiener filter, and the results are shown in Fig. 4. Because Fig. 1(b) reflects the preset displacement distribution of our synthetic supercells, it can be regarded as the standard and undistorted displacement distribution. Therefore, the more the calculated results in Fig. 4 deviate from those in Fig. 1(b), the larger is the displacement distortion caused by the Wiener filter. The calculated displacement distribution can be intuitively seen to have been distorted when the amorphous carbon layer was added. The distortion is larger when the amorphous layer is thicker, and the distortion is also large when using the 90% quantile fractile as the estimate parameter.

Now we already have some basic understanding of the effect of a Wiener filter in such a system. In order to analyze quantitatively the effect of the Wiener filter, some statistic parameters need to be defined for further comparisons.

For each B-site ion (i, j) in the i^{th} row and on the j^{th} line, the displacement vector can be denoted as $\boldsymbol{P_{ij}} = (P_{ijx}, P_{ijy})$, and its length L_{ij} and angle A_{ij} can be calculated as

$$L_{ij} = \sqrt{P_{ijx}^2 + P_{ijy}^2}, \quad A_{ij} = \arctan\Big(\frac{P_{ijy}}{P_{ijx}}\Big). \tag{18}$$

If L_{ij}^* and A_{ij}^* are the corresponding values for ion (i, j) in the original model without amorphous carbon layer, then three statistics can be defined:

$$\begin{cases} \overline{L_a} = \dfrac{1}{100}\displaystyle\sum_{i,j} |L_{ij} - L_{ij}^*|, \\ \overline{L_r} = \dfrac{1}{100}\displaystyle\sum_{i,j} \dfrac{|L_{ij} - L_{ij}^*|}{L_{ij}^*}, \\ \overline{A} = \dfrac{1}{100}\displaystyle\sum_{i,j} |A_{ij} - A_{ij}^*|. \end{cases} \tag{19}$$

Here, $\overline{L_a}$, $\overline{L_r}$, and $\overline{A}$ are the average absolute length deviation (the unit is pm), the average relative length deviation, and the average angle deviation, respectively. Table 2 shows the corresponding statistics.

As shown in Table 2, after a Wiener filter with a small estimate parameter, namely, a 30% and a 50% quantile fractile is taken, both the average length deviation and the average angle deviation are decreased compared with the values for the unprocessed images; this can be explained by the fact that the Wiener filter undermines the effect of the amorphous layer. However, a large estimate parameter, such as a 90% quantile fractile, causes larger distortion because a large quantile fractile means that only a small part of the frequency domain information can be used, resulting in the loss of original lattice information.

In practical experiments, the amorphous layer usually is not very thick, and the corresponding noise is not very strong. If we take 4 nm as the upper thickness limit of the amorphous carbon layer and consider HRTEM images with aperiodic ferroelectric displacement, the average relative length deviation of the displacement vector obtained by Wiener filter with moderate parameters will be controlled below 12%, and the average angular deviation of the displacement vector will be within 5°.

Here, we give a brief description of this work. First of all, contrary to our customary thinking, synthetic experiments showed that with proper parameters, a Wiener filter will not decrease the accuracy of the displacement measurement, which is helpful for further investigation of an experimental system with an amorphous layer. Secondly, they give an error bar for the determination of the atomic displacement in the HRTEM image, which is important for our quantitative analysis, such as acting as a criterion to determine whether the local ferroelectric polarization is changed in in-situ experiments: according to the previous discussion, the error bar of the quantitative measurement of the displacement after a Wiener filter can be estimated as 12%. If the measured value of average relative length deviation $\overline{L_r}$ before and after changing an external electric field is more than $\sqrt{2} \times 12\% \approx 17\%$, then the assertation that external electric field does change the local ferroelectric state is reasonable.

IV. CONCLUSION

When an experimental system contains both aperiodic ionic displacements and an amorphous layer, using a Wiener filter with a moderate parameter can significantly improve the SNR, while the accuracy of the displacement measurement will not decrease, which means that the information of the aperiodic displacement can be well preserved. If the thickness of the amorphous layer is not more than 4 nm, the average relative length deviation will be controlled to be below 12%, and the average angular deviation of the displacement vector to be within

5° after the Wiener filter. Such results are useful for both quantitatively calculating the ferroelectric displacement in a HRTEM image and may guide some experiments based on atomic observation, such as analyzing in-situ experimental results obtained under an external electric field.

ACKNOWLEDGMENTS

We would like to thank R. Kilaas for his detailed discussion about the Wiener filter, and R. Yu for providing amorphous carbon models. This work was financially supported by the Chinese National Natural Science Foundation (11374174, 51390471, and 51527803), the National 973 Project of China (2015CB654902) and the National Key Research and Development Program (2016YFB0700402). This work made use of the resources of the National Center for Electron Microscopy in Beijing.

REFERENCES

[1] R. Yu *et al.*, Phys. Rev. Lett. **105**, 226101 (2010).
[2] M. R. He, R. Yu and J. Zhu, Nano Lett. **12**, 704 (2012).
[3] S. Q. Deng *et al.*, ACS Appl. Mater. Interfaces **9**, 27322 (2017).
[4] L. H. Liu *et al.*, Sci. Bull. **63**, 1570 (2018).
[5] C. L. Jia *et al.*, Nat. Mat. **7**, 57 (2008).
[6] P. Gao *et al.*, Nat. Commun. **4**, 2791 (2013).
[7] J. Seidel *et al.*, Nat. Mat. **8**, 229 (2009).
[8] G. Catalan *et al.*, Nat. Mat. **10**, 963 (2011).
[9] Y. L. Tang *et al.*, Sci. Rep. **4**, 4115 (2014).
[10] C. T. Nelson *et al.*, Nano Lett. **11**, 828 (2011).
[11] C. L. Jia *et al.*, Science **331**, 1420 (2011).
[12] Y. L. Tang *et al.*, Science **348**, 547 (2015).
[13] A. K. Yadav *et al.*, Nature **530**, 198 (2016).
[14] L. Xie *et al.*, Phys. Rev. B **85**, 014118 (2012).
[15] T. Shi, L. Xie, L. Gu and J. Zhu, Sci. Rep. **5**, 8606 (2015).
[16] F. Li *et al.*, Nat. Mat. **17**, 349 (2018).
[17] C. L. Jia *et al.*, Nat. Mat. **6**, 64 (2007).
[18] Y. L. Li *et al.*, J. Am. Ceram. Soc. **98**, 2710 (2015).
[19] L. X. Zhang *et al.*, Science **361**, 494 (2018).
[20] R. Kilaas, J. Microscopy **190**, 45 (1998).
[21] H. Wang *et al.*, J. Am. Ceram. Soc. **91**, 2382 (2008).
[22] R. Yu, M. Lentzen and J. Zhu, Ultramicroscopy **112**, 15 (2012).